10.1098/rspa.2003.1225

THE ROYAL SOCIETY

Kinetics of the bainite transformation

By Hiroshi Matsuda† and Harshad K. D. H. Bhadeshia

Department of Materials Sciences and Metallurgy, University of Cambridge, Pembroke Street, Cambridge CB2 3QZ, UK (hkdb@cus.cam.ac.uk)

Received 15 November 2002; accepted 13 August 2003; published online 16 March 2004

A theory is developed for the evolution of bainite as a function of time, temperature, chemical composition and austenite grain size. The model takes into account the details of the mechanism of transformation, including the fact that nucleation begins at the austenite grain surfaces, and that the growth of a sheaf occurs by the repeated nucleation of small platelets. Predictions made using the model are shown to compare well against published isothermal and continuous cooling transformation data.

Keywords: steel; bainite; kinetics; modelling; isothermal transformation; continuous cooling transformation

1. Introduction

Bainite represents one of the most fertile areas of steel research and development: transformation-assisted steels for automotive applications, inoculated acicular ferrite steels for the construction of oil platforms, high-strength alloys for the defence and aerospace industries, ultra-low carbon bainitic steels for the construction industries, etc. (Bhadeshia 2001). There has also been a great deal of progress in understanding the mechanism of the bainite reaction so it is timely to encapsulate this knowledge into a quantitative model of use in the design of new steels. This is the purpose of the present work and we begin with a summary of the essential foundations of the model. As explained in a recent review (Bhadeshia 1999), there are still unresolved issues about the nature of the bainite reaction, but it is nevertheless worth emphasizing that the mechanism summarized below is the only one which has led to the design of novel alloys (Caballero *et al*. 2001*a*, *b*, 2002). On the basis of accumulated evidence (Bhadeshia 2001), the present work assumes a displacive mechanism of transformation which determines the morphology of the bainite plates, the shape deformation accompanying transformation, and the transformation thermodynamics which influence the extent of reaction. A different scenario, in which the plate of bainite grows by a ledge mechanism, with the uncoordinated passage of atoms across the transformation interface, has also been proposed (Hehemann *et al*. 1972) but does not lend itself to a quantitative treatment since there is no theory proposed for the frequency and height of the ledges. The details of the various mechanisms have been reviewed elsewhere (Bhadeshia 2001).

† Present address: Steel Research Laboratory, JFE Steel Corporation, 1 Kokan-cho Fukuyama, Hiroshima-Prefecture 721-8510, Japan (h-matsuda@jfe-steel.co.jp).

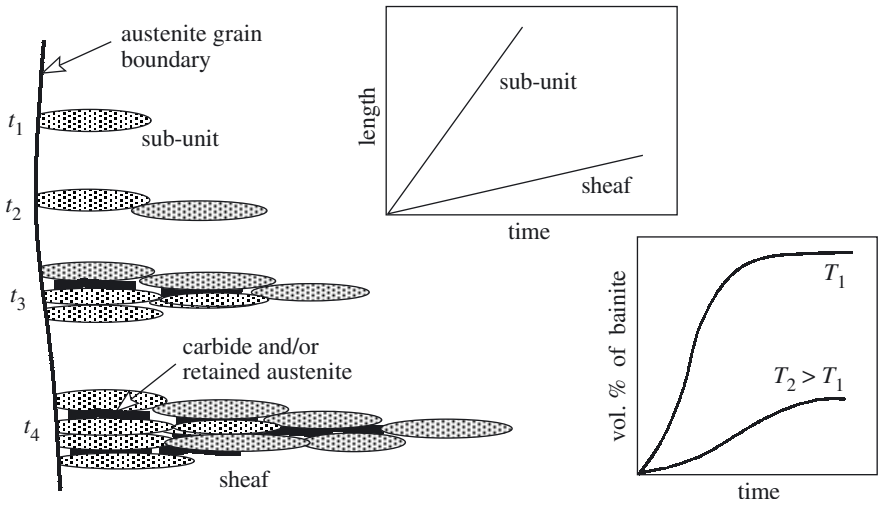

Figure 1. The microstructural features relevant in the kinetic description of a bainitic microstructure. There is the lengthening of sub-units (individual platelets) and of sheaves (clusters of platelets), the latter by the repeated nucleation of sub-units, the precipitation of carbides and the change in volume fraction as a function of time and temperature.

2. Previous kinetic models

Oblak & Hehemann (1967) first suggested that the bainite reaction proceeds in a stepwise manner by the martensitic formation of individual platelets, each of which grows to a limited size; the details have been reviewed by Hehemann (1970). The transformation is therefore propagated by the nucleation of new platelets. This visionary idea laid the foundations for the development of thermodynamic and kinetic theory on the basis of transformation mechanism rather than empirical fitting to experimental data.

The first theory based on the mechanism of the bainite reaction, which emerged in 1982 (Bhadeshia 1982*a*), incorporated the following principles.

(i) An individual platelet grows without diffusion. Any excess carbon is then partitioned into the residual austenite (Bhadeshia & Edmonds 1980). The limiting fraction of bainite at any temperature is determined by the condition that the free energies of austenite and ferrite of the same composition become identical.

(ii) The size of each platelet is limited by a breakdown in interface coherency due to the plastic accommodation of the shape deformation (Bhadeshia & Edmonds 1979). The growth of a cluster of platelets therefore requires the nucleation of new platelets.

(iii) Classical nucleation theory is inappropriate for the bainite reaction (Bhadeshia 1981). Nucleation is governed instead by the dissociation of three-dimensional arrays of dislocations.

This theory (Bhadeshia 1982*a*) was able to reproduce important features of the bainite transformation in carbide-free steels, for example, the fact that the bainite start temperature (B_S) is far below that at which ferrite formation becomes thermodynamically possible. The essential kinetic features of the bainite transformation are

illustrated schematically in figure 1. The first applications of the theory began some 10 years later, when it was realized by Rees & Bhadeshia (1992*a*, *b*) that there was a mathematical difficulty which caused the model to incorrectly represent alloying element effects. Singh & Bhadeshia then incorporated the influence of strain on the kinetics of transformation (Singh & Bhadeshia 1996, 1998; Singh 1998). Because of the complexity of the mathematical equations, the solutions were obtained numerically, but Chester & Bhadeshia (1997) later proved that an analytical solution is also possible; this work has been exploited by Thomson *et al*. (2000) in dealing with austempered ductile cast irons.

Apart from the work described above, there is no theory in the published literature which accounts for the mechanism of bainite. Following earlier work by Hillert, Ågren (1989) attempted to treat Widmanstätten ferrite, bainite and martensite in a grand model, which is, however, unphysical. In particular, the plate shape itself is lost at high supersaturations. A recent theory by Quidort & Brechet (2001) fails to account for the microstructure of bainite and the major strains associated with transformation, and treats the entire process in terms of diffusion-controlled growth, even though the growth rate of individual platelets of bainite has been observed to be many orders of magnitude in excess of that predicted by diffusion-controlled growth. Another recent model by Tszeng (2000) is conceptually flawed in its treatment of extended volume. All the available theory has been reviewed in Bhadeshia (2001).

One of the main drawbacks of the kinetic theory by Bhadeshia and co-workers is that the model does not distinguish between the initial nucleation events at the austenite grain surfaces and those that follow autocatalytically to generate the sheaf microstructure. The model essentially considers nucleation to occur at random, which it clearly does not. It is therefore not possible to properly represent the austenite grain size effect, nor to treat the evolution of the shape of bainite sheaves. These and other features are incorporated in the model described here.

3. Development of model

(*a*) *Thermodynamics of bainite Formation*

It has been demonstrated that bainite does not follow classical nucleation theory involving heterophase fluctuations, but rather follows a theory similar to that of martensite where the activation energy for nucleation is related directly to the driving force (Bhadeshia 1981, 1982*b*). The formation of bainite becomes possible at a temperature where the conditions for nucleation and growth are satisfied simultaneously. To achieve a detectable nucleation rate,

$$\Delta G_{\mathrm{m}} < G_{\mathrm{N}}, \tag{3.1}$$

where ΔG_{m} is the maximum free energy available for para-equilibrium nucleation in which only carbon is partitioned between the parent and product phases. G_{N} is a universal nucleation function which expresses the minimum free energy required to obtain a detectable amount of Widmanstätten ferrite or bainite. ΔG_{m} is calculated using the parallel tangent construction as described in Bhadeshia (1982*b*). G_{N} has been determined experimentally as (Ali & Bhadeshia 1990):

$$G_{\mathrm{N}} = 3.637(T - 273.15) + 2540 \text{ J mol}^{-1}, \tag{3.2}$$

where T is the absolute temperature.

The nucleus can only evolve into bainite if there is sufficient driving force available for growth without a composition change, after accounting for the stored energy due to the shape deformation (Ko & Cottrell 1952; Bhadeshia 1981; Bhadeshia & Christian 1990). The latter has been estimated to be *ca.* 400 J mol^{-1} (Bhadeshia 1981; Bhadeshia & Christian 1990), so that the condition for growth becomes

$$\Delta G^{\gamma\rightarrow\alpha} < -400 \text{ J mol}^{-1}, \tag{3.3}$$

where $\Delta G^{\gamma\rightarrow\alpha}$ is the free-energy change for the transformation of austenite into ferrite of the same composition, calculated as in Bhadeshia (1982*b*). This condition also sets the limiting fraction $V_\beta^{\max}$ of bainitic ferrite that can form at any temperature

$$V_\beta^{\max} = \frac{x_{T_0'} - \bar{x}}{x_{T_0'} - x^{\alpha\gamma}}, \tag{3.4}$$

where $\bar{x}$ is the average carbon concentration of the steel, $x^{\alpha\gamma}$ is the para-equilibrium carbon concentration of the ferrite and $x_{T_0'}$ is the carbon concentration corresponding to the T_0' (the T_0 corrected for stored energy). $x_{T_0'}$ and $x^{\alpha\gamma}$ are also calculated as in Bhadeshia (1982*b*).

The thermodynamic parameters such as ΔG_{m}, $\Delta G^{\gamma\rightarrow\alpha}$, $x_{T_0'}$ and $x^{\alpha\gamma}$ change during transformation as the austenite enriches with carbon. This is taken into account by updating the chemical composition of the residual austenite during each time-step of the calculation; this assumes that the carbon is homogeneously distributed in the austenite, a procedure known as the 'mean field approximation'.

(i) *Grain-boundary nucleation*

There are two processes to consider in the evolution of the bainitic microstructure, the independent nucleation of a sub-unit at an austenite grain surface and the subsequent autocatalytic nucleation of sub-units on pre-existing platelets. The latter process is essential in the generation of the sheaf structure, whereas the former incorporates an austenite grain size effect on the overall transformation kinetics. The nucleation rate, I, is dependent on the activation energy as

$$I \propto \nu \exp\left\{-\frac{G^*}{RT}\right\}, \tag{3.5}$$

where $\nu = k_{\mathrm{B}}T/h$ is the attempt frequency factor, k_{B} and h are the Boltzmann and Planck constants respectively, G^* is the activation energy for nucleation, and R is the universal gas constant.

The activation energy for the nucleation of bainite is proportional to the driving force for transformation (Bhadeshia 1981), consistent with the theory for martensite nucleation (Magee 1970; Olson & Cohen 1976*a*–*c*), although for bainite and Widmanstätten ferrite the carbon must be allowed to partition during nucleation (Bhadeshia 1981). By contrast, martensitic nucleation is diffusionless. Therefore, the nucleation rate per unit area of austenite grain boundary is written

$$I_{\mathrm{g}} = K_1\nu \exp\left\{-\frac{K_2 + K_3'\Delta G_{\mathrm{m}}}{RT}\right\} = K_1\nu \exp\left\{-\frac{K_2}{RT}\left(1 + \frac{\Delta G_{\mathrm{m}}}{K_3}\right)\right\}, \tag{3.6}$$

where K_i are constants with $K_3 = 2540 \text{ J mol}^{-1}$ (Bhadeshia 1982*a*; Rees & Bhadeshia 1992*a*).

K_1 and K_2 are calculated using published data as follows. It is assumed that the initial stages of transformation are controlled purely by nucleation events at the austenite grain surfaces and that autocatalysis can be neglected. The volume of bainitic ferrite, V_β, can then be related to the grain-boundary nucleation rate,

$$V_\beta = V_\mathrm{u} S_\mathrm{V} I_\mathrm{g} t, \tag{3.7}$$

where each nucleus transforms to a finite volume V_u of a sub-unit, S_V is the austenite grain-boundary surface per unit volume, and t is the elapsed time since the start of transformation. It is known from standard stereology that $S_\mathrm{V} = 2/\bar{L}$, where $\bar{L}$ is the mean lineal intercept measure of the austenite grain size.

There have been many studies of the thickness of bainite sub-units (Bhadeshia & Edmonds 1979; Singh & Bhadeshia 1998; Singh 1998; Chang & Bhadeshia 1995), but the volume per platelet has never been measured. It is sometimes assumed that this volume is constant at $0.2 \times 10 \times 10\ \mu\mathrm{m}^3$, where the plate thickness is $0.2\ \mu\mathrm{m}$ and length $10\ \mu\mathrm{m}$ (Bhadeshia 1982*a*; Rees & Bhadeshia 1992*a*, *b*) but this is clearly unsatisfactory given the known refinement of the microstructure when the transformation temperature is reduced. Parker (1997) has empirically modelled the thickness as $0.2 \times (T - 528)/150\ \mu\mathrm{m}$, based on experimental data by Chang & Bhadeshia (1995), for steels containing 0.095–0.5 wt % C, transformed isothermally between 523 and 773 K. If it is assumed that all the dimensions scale with temperature in this way, then it follows that the sub-unit volume is given by

$$\begin{aligned} V_\mathrm{u} &= \left(10.0 \times 10^{-6} \times \frac{T - 528}{150}\right)^2 \times 0.2 \times 10^{-6} \times \frac{T - 528}{150} \\ &= 2.0 \times 10^{-17} \times \left(\frac{T - 528}{150}\right)^3 \mathrm{m}^3. \end{aligned} \tag{3.8}$$

(ii) *Growth of sheaves*

Given that individual sub-units grow much more rapidly than sheaves (Ali & Bhadeshia 1989), the lengthening rate of the sheaf is determined by the interval between successive sub-unit autocatalytic-nucleation events. If a sub-unit reaches its limiting size in a time-interval, t_u, and another one nucleates at the tip of the original sub-unit after the time-interval, Δt_s, then the overall lengthening rate of a sheaf, v_s, is given by (Ali & Bhadeshia 1989; Bhadeshia 1990)

$$v_\mathrm{s} = \frac{v_\mathrm{u} t_\mathrm{u}}{t_\mathrm{u} + \Delta t_\mathrm{s}}, \tag{3.9}$$

where v_u is the average lengthening rate of a sub-unit. Since $t_\mathrm{u} \ll \Delta t_\mathrm{s}$ equation (3.9) can be rewritten as

$$v_\mathrm{s} \simeq \frac{l_\mathrm{u}}{\Delta t_\mathrm{s}}. \tag{3.10}$$

The rate with which successive sub-units, I_s, can be described in the same manner as equation (3.5) through (3.6), so that

$$I_\mathrm{s} = K_4' \nu \exp\left\{-\frac{K_5}{RT}\left(1 + \frac{\Delta G_\mathrm{m}}{K_3}\right)\right\}, \tag{3.11}$$

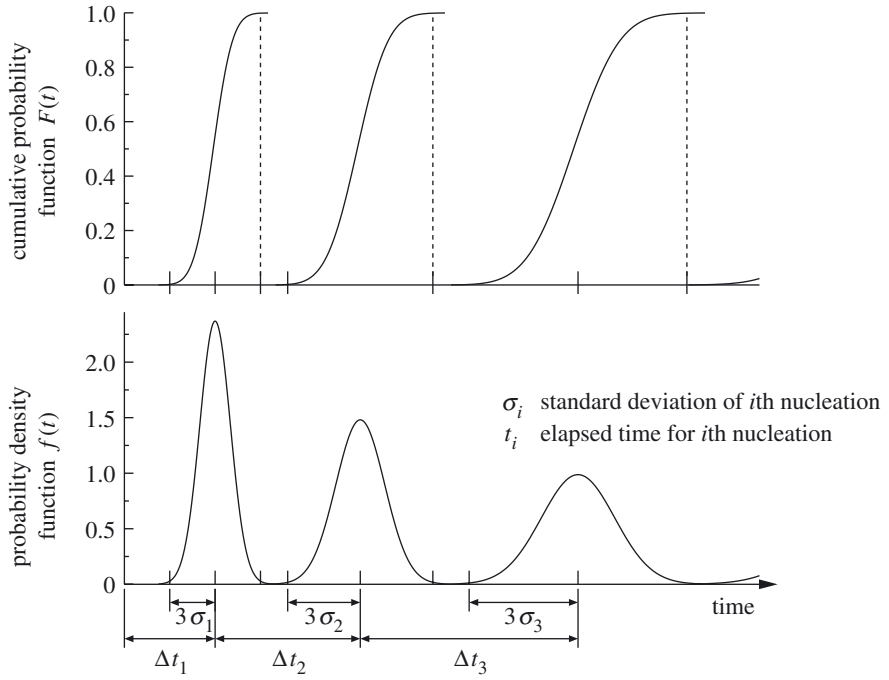

Figure 2. Schematic of the distribution of elapsed time for the nucleation of successive sub-units in this model.

and therefore

$$\Delta t_{\mathrm{s}} = \frac{1}{I_{\mathrm{s}}} = \frac{K_4}{\nu} \exp\left\{ \frac{K_5}{RT}\left(1 + \frac{\Delta G_{\mathrm{m}}}{K_3}\right)\right\}, \tag{3.12}$$

where K_4 and K_5 are fitting constants evaluated numerically in the same manner as the previous research (Rees & Bhadeshia 1992*a*).

Although the elapsed time is identical for all sub-units that nucleated at the same instance in time, it is improbable that all the sheaves initiate at the same time and grow in precisely the same manner, since the spatial location will to some extent introduce noise. Therefore, the actual interval between successive sub-units is assumed to be Gaussian distributed with the mean of the calculated elapsed time and standard deviation of 1/6 of that, as illustrated schematically in figure 2. Note that the mean elapsed time is expected to increase during transformation as the chemical composition of the austenite changes.

(*b*) *Overall transformation kinetics*

In order to explicitly deal with grain-boundary nucleation, Cahn (1956) adapted the Johnson & Mehl (1939), Avrami (1939, 1940, 1941) and Kolmogorov concept of extended volume to extended area. Extended space is simply that in which particles can grow through each other and nucleate in regions which have already transformed. Counting all parts of extended space therefore leads to an erroneous estimate of the actual amount of transformation: an error which can be corrected by scaling extended space by the probability that an increment of transformation falls in a previously untransformed matrix.

Consider a planar grain boundary upon which a phase α nucleates randomly and hence consumes some of the grain-boundary area. The change in extended grain-boundary area $\mathrm{d}O_\alpha^{\mathrm{e}}$ is then related to the change in real grain-boundary area $\mathrm{d}O_\alpha$ by

$$\mathrm{d}O_\alpha = \left(1 - \frac{O_\alpha}{O_{\mathrm{B}}}\right) \mathrm{d}O_\alpha^{\mathrm{e}}, \tag{3.13}$$

so that

$$\frac{O_\alpha}{O_{\mathrm{B}}} = 1 - \exp\left(-\frac{O_\alpha^{\mathrm{e}}}{O_{\mathrm{B}}}\right), \tag{3.14}$$

where O_{B} is the total area of grain boundary in whole assembly.

Consider now a test-plane parallel to the boundary and a distance y away from it. Particles nucleated at the boundary will intersect this plane with a different extended area. By integrating these extended areas as a function of y, it is possible to obtain the extended volume V_α^{e} due to particles growing from grain boundaries:

$$V_\alpha^{\mathrm{e}} = \int_{y=-\infty}^{\infty} O_\alpha \,\mathrm{d}y = O_{\mathrm{B}} \int_{y=-\infty}^{\infty} \left\{1 - \exp\left(-\frac{O_\alpha^{\mathrm{e}}}{O_{\mathrm{B}}}\right)\right\} \mathrm{d}y. \tag{3.15}$$

The volume fraction, ψ_α, of precipitated phase α at the time t is then obtained by converting the extended volume into the real volume as

$$\mathrm{d}V_\alpha = \left(1 - \frac{V_\alpha}{V_{\mathrm{T}}}\right) \mathrm{d}V_\alpha^{\mathrm{e}}, \tag{3.16}$$

so that

$$\psi_\alpha = \frac{V_\alpha}{V_{\mathrm{T}}} = 1 - \exp\left(-\frac{V_\alpha^{\mathrm{e}}}{V_{\mathrm{T}}}\right), \tag{3.17}$$

where V_{T} is the total volume of the system.

These equations must in practice be implemented numerically to allow for changing boundary conditions as transformation proceeds (Jones 1996; Jones & Bhadeshia 1997*a*, *b*). The discretized form of (3.13) is

$$\Delta O_{\beta,y} = \left(1 - \frac{O_{\beta,y}}{O_{\mathrm{B}}}\right) \Delta O_{\beta,y}^{\mathrm{e}}, \tag{3.18}$$

where $O_{\beta,y}$ and $O_{\beta,y}^{\mathrm{e}}$ are the real area and the extended area of bainite intersected with the plane at distance y from the grain boundary, respectively.

The extended area has contributions from all sub-units nucleated from the start of transformation to $t = m\Delta t$, where m is an integer such that $m\Delta t$ is the current time t. Therefore, the change in the extended area becomes

$$\Delta O_{\beta,y}^{\mathrm{e}} = \sum_{k=0}^{m} E_{k,m,y} O_{\mathrm{B}} I_{B,k} \Delta\tau, \tag{3.19}$$

where $E_{k,m,y}$ is the change in area on plane y intersected by the new phase, which nucleated between $k\Delta\tau$ and $(k+1)\Delta\tau$ on the boundary, during the current time-interval $m\Delta t$ to $(m+1)\Delta t$. $I_{B,k}$ is the nucleation rate per unit area of bainite during the same time-interval. The expression $O_{\mathrm{B}} I_{B,k} \Delta\tau$ represents the number of extended particles nucleated in the same time-interval. Note that Δt and $\Delta\tau$ are numerically

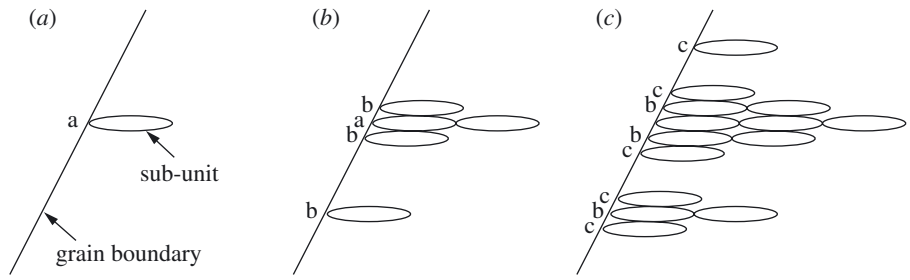

Figure 3. Schematic illustrating the growth of sheaves by propagation of successive sub-units.

identical. This expression differs from the work of Jones & Bhadeshia (Jones 1996; Jones & Bhadeshia 1997*a*, *b*) because the bainite transformation propagates by the intermittent nucleation of sub-units.

Therefore, the change in real area of bainite, $\Delta O_{\beta,y}$, during the time-interval t to $t+\Delta t$ is determined by substituting equation (3.19) into equation (3.18), which is then used to update the total area, $O_{\beta,y,t+\Delta t}$, intersected by the bainite within a plane y at the time $t+\Delta t$ as

$$O_{\beta,y,t+\Delta t} = O_{\beta,y,t} + \Delta O_{\beta,y}. \tag{3.20}$$

Bainite grows with the coordinated movement of atoms and hence cannot cross austenite grain boundaries. The change in the extended volume of bainite in the time-interval t to $t+\Delta t$ is, therefore, obtained by integrating the change in real area numerically as

$$\Delta V_\beta^{\mathrm{e}} = \Delta y \sum_{y=0}^{q^{\max}} \Delta O_{\beta,y}, \tag{3.21}$$

where Δy is a small interval in y and $q^{\max}$ is the maximum length of the bainite sheaves. Here, the change in the real volume of bainite, V_β, at the time t can be described numerically in the same manner as equation (3.16), so that

$$\Delta V_\beta = \left(1 - \frac{V_\beta}{V_{\mathrm{T}}}\right) \Delta V_\beta^{\mathrm{e}}. \tag{3.22}$$

This instantaneous value of ΔV_β can be used to update the total real volume of bainite at the time $t+\Delta t$:

$$V_{\beta,t+\Delta t} = V_{\beta,t} + \Delta V_\beta. \tag{3.23}$$

(i) *Changes in sheaf length and the extended area*

In order to apply the numerical procedure described above to the bainite transformation, the changes in sheaf length and extended area at each time-step are required. Sheaves grow intermittently (see figure 3).

The change in length of a sheaf, which nucleated in the interval $k\Delta\tau$ to $(k+1)\Delta\tau$, during the current time-interval $m\Delta t$ to $(m+1)\Delta t$ is given by

$$\Delta q_k = \begin{cases} 0 & [(m+1)\Delta t - n_k \Delta t < \Delta t_{\mathrm{s}}], \\ l_{\mathrm{u}} & [(m+1)\Delta t - n_k \Delta t \geqslant \Delta t_{\mathrm{s}}], \end{cases} \tag{3.24}$$

Table 1. *Chemical compositions and mean linear intercept values analysed in this study*
(Mean linear intercept values represent austenite grain size.)

	chemical compositions (wt %)							mean linear intercept
steel	C	Si	Mn	Ni	Mo	Cr	V	(μm)
1	0.22	2.03	3.00	0.00	0.00	0.00	0.00	47 ± 5
2	0.39	2.05	0.00	4.08	0.00	0.00	0.00	25 ± 6
3	0.44	1.74	0.67	1.85	0.83	0.39	0.09	86 ± 9

where $n_k\Delta t$ is the time at which the last nucleation event occurred. The value of $n_k\Delta t$ is updated to $n_k\Delta t = (m+1)\Delta t$ when another nucleation event occurs. The length of the sheaf is similarly updated:

$$q_{k,(m+1)\Delta t} = q_{k,m\Delta t} + \Delta q_k. \tag{3.25}$$

The extended area due to the intersection of a sheaf with a test plane also changes intermittently because the thickening of sheaves is controlled by the nucleation of sub-units. The change in the extended area on plane y of a sheaf of bainite nucleated at the time-interval between $k\Delta\tau$ and $(k+1)\Delta\tau$, during the current time-interval $m\Delta t$ to $(m+1)\Delta t$, is given as

$$E_{k,m,y} = \begin{cases} S_{\mathrm{u}} & [n_k\Delta t = (k+1)\Delta\tau], \\ 0 & [(m+1)\Delta t - n_k\Delta t < \Delta t_{\mathrm{s}}], \\ \theta S_{\mathrm{u}} & [(m+1)\Delta t - n_k\Delta t \geqslant \Delta t_{\mathrm{s}}], \end{cases} \tag{3.26}$$

where θ is the autocatalysis factor, which, unlike in previous work (Bhadeshia 1982*a*; Rees & Bhadeshia 1992*a*, *b*), is taken as 2.0 in order to preserve the shape of the sheaf.

The numerical procedure outlined here permits the composition of the austenite to be modified as bainite forms, and is applicable to both isothermal and anisothermal transformation.

4. Results and discussion

(*a*) *Determination of fitting parameters*

Published experimental data (Bhadeshia 1982*a*; Rees & Bhadeshia 1992*a*) are here interpreted and used to determine the experimental constants. The chemical compositions and the mean linear intercept values for the austenite grain size of the steels are given in table 1. Mean linear intercept values were measured after austenitization for 300 s at 1273 K; a procedure is detailed in Rees & Bhadeshia (1992*a*).

Figure 4 shows experimentally determined isothermal transformation curves for the three steels (Bhadeshia 1982*a*). The transformation curves were obtained by measuring dilatational length changes (Bhadeshia 1982*a*). These data give the appearance of including rogue results, especially in steels 1 and 2. Therefore, discrimination is needed to evaluate rational determination of the experimental constants.

Figure 5 shows the calculated $V_{T_0'}$ curves for the steels and plots of maximum volume fraction in the experimental data of each condition. The curves are calculated

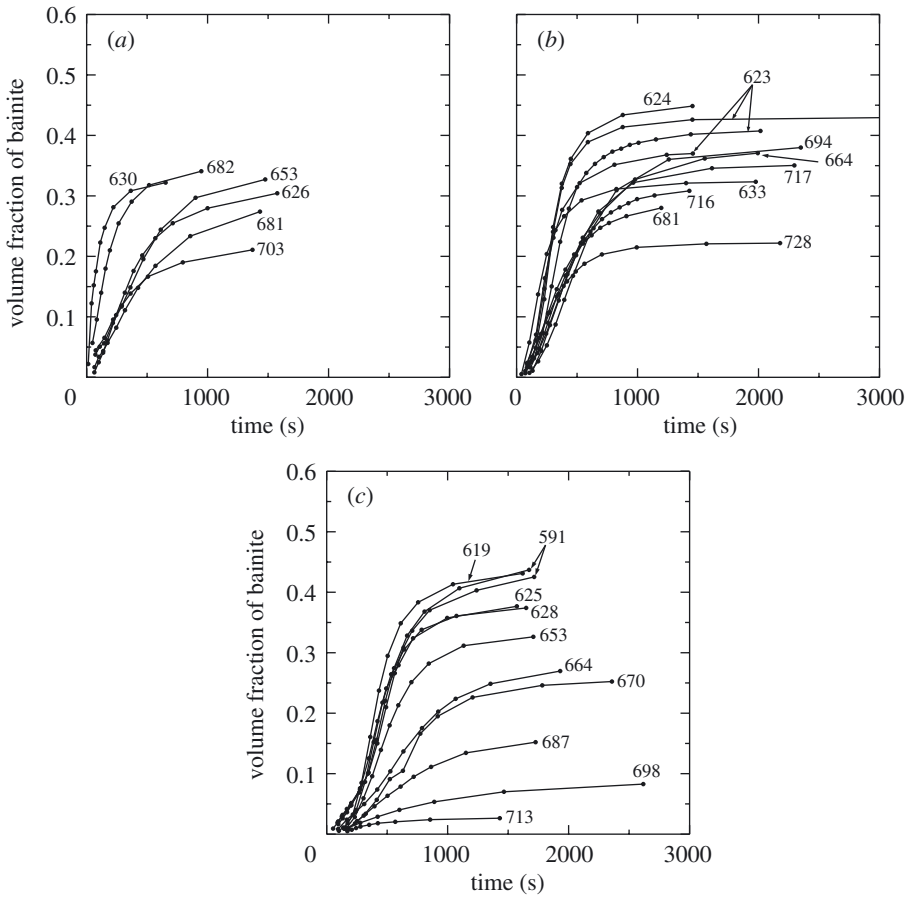

Figure 4. Experimentally determined isothermal transformation curves: (*a*) steel 1; (*b*) steel 2; (*c*) steel 3.

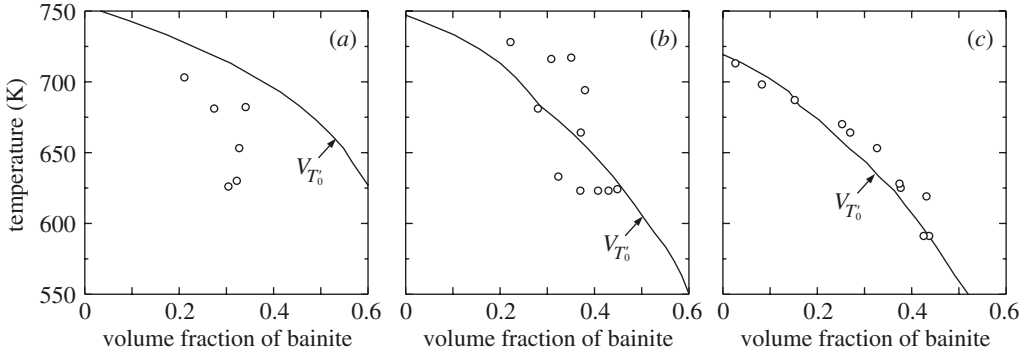

Figure 5. The solid curve represents the calculated relationship between temperature and maximum volume fraction of bainite, and open symbols indicate the maximum volume fraction of experimental results: (*a*) steel 1; (*b*) steel 2; and (*c*) steel 3.

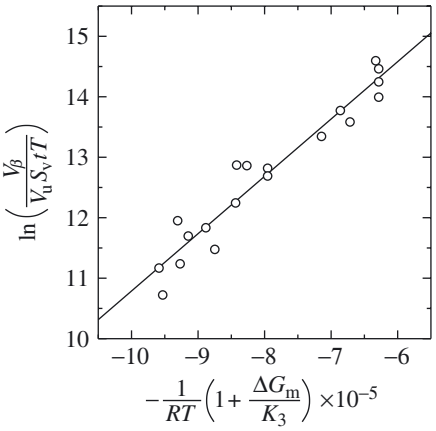

Figure 6. The relationship between parameters associated with equation (3.7).

from equation (3.4) over the temperature. The plots of maximum volume fraction are assumed to be the saturated value, and are used to rationalize the data by comparing them with the $V_{T_0'}$ curves. Steel 3 represents the most consistent behaviour, as bainite transformation ceases when the volume fraction reaches $V_{T_0'}$ of three steels. The other two steels, however, include eccentric results; in particular, all the plots of steel 1 are significantly small compared with the $V_{T_0'}$ curve. It is obviously impossible for the value of the volume fraction to reach $V_{T_0'}$, even when the transformation curves are extrapolated up to *ca.* 5000 s. Therefore, all the data of steel 1 are discarded from the calculation used to determine the experimental constants.

K_1 and K_2 are determined first. Equation (3.7) is valid only in the initial stages of transformation in which there is no sub-unit formed by the autocatalysis, and thus only the data for which the volume fraction of bainite is less than 0.001 were chosen to apply the evaluation. Figure 6 shows the relationship between parameters related with equation (3.7). This relationship indicated very good agreement, and thus K_1 and K_2 were taken as 3.049×10^{-2} m^{-2} s^{-1} and 9.481×10^4 J mol^{-1}, respectively. Furthermore, this assumption is reasonable because the elapsed time to nucleate the next sub-unit by autocatalysis is between 10 seconds and several hundred seconds, as described later, and all elapsed times for the data used here are less than those results.

K_4 and K_5 are then optimized to give the best agreement between the theory and the experimental data. Thus, K_4 and K_5 were taken as 1.663×10^{13} and 6.233×10^4 J mol^{-1}, respectively.

(*b*) *Application of the model*

Some examples of calculated and experimentally determined isothermal transformation curves are shown in figure 7. It is demonstrated that the model is generally capable of predicting the transformation kinetics accurately. Although the predicted curve is inconsistent with the experimental one at 728 K in steel 2, this is because of the discrepancy between the calculated and experimental $V_{T_0'}$ as shown in figure 5*b*. In steel 3, there is a certain discrepancy of kinetics at 591 K. This may arise from the formation of lower bainite, which is not addressed in this model, because it

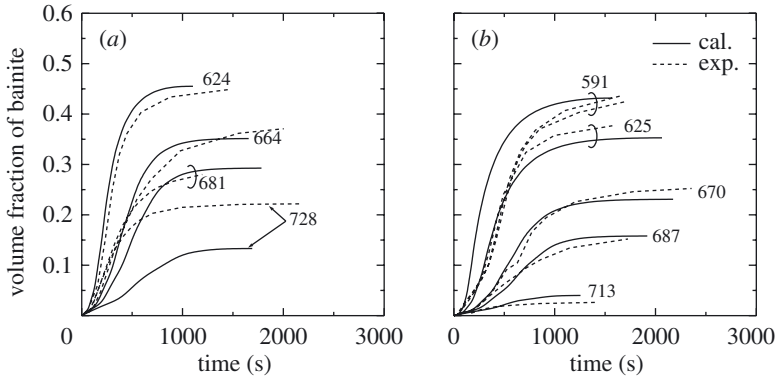

Figure 7. Comparison of calculated and experimentally determined isothermal transformation curves: (*a*) steel 2; (*b*) steel 3.

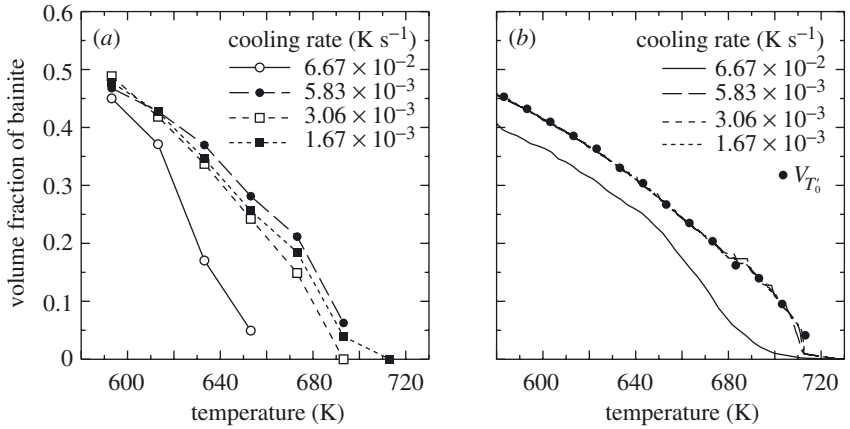

Figure 8. Relationship between temperature and the volume fraction of bainite in continuous cooling transformation of steel 3. (*a*) Experimentally determined values (Khan & Bhadeshia 1990). (*b*) Values calculated using the present model.

was reported that carbide-free upper bainite was obtained above 593 K but a small amount of lower bainite was observed at 593 K (Khan & Bhadeshia 1990).

Changes in experimental and calculated volume fractions of bainite during continuous cooling are shown in figure 8. Experimental results were determined by Khan & Bhadeshia (1990). Calculated $V_{T_0'}$ points are also plotted in figure 8*b*. Figure 9 shows experimental and calculated continuous cooling transformation curves of steel 3. Experimental curves are evaluated by interpolating the Khan & Bhadeshia results (1990); the experimental 1% curve is not available, although that calculated is presented in figure 9*b*. Trends of the transformation are clearly well represented by the model, although calculated results predict a relatively large amount of volume fraction at high temperature and small amount at low temperature compared with the experimental results. It is found from figure 8*b* that transformations are retarded by $V_{T_0'}$ in the three slower conditions; on the other hand, transformation does not saturate at each temperature during cooling in the fastest cooling condition.

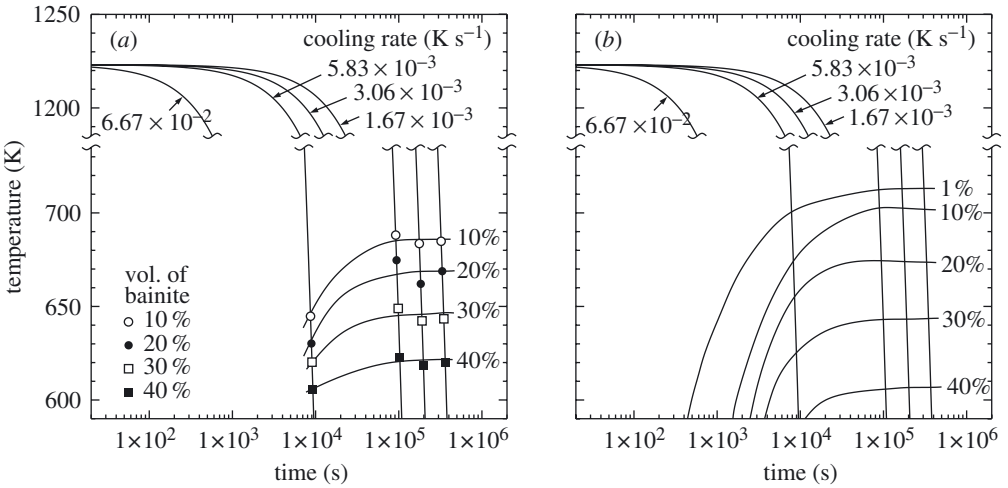

Figure 9. Continuous cooling transformation curves of steel 3: (*a*) evaluated by interpolating the experimental data by Khan & Bhadeshia (1990); (*b*) calculated using this model.

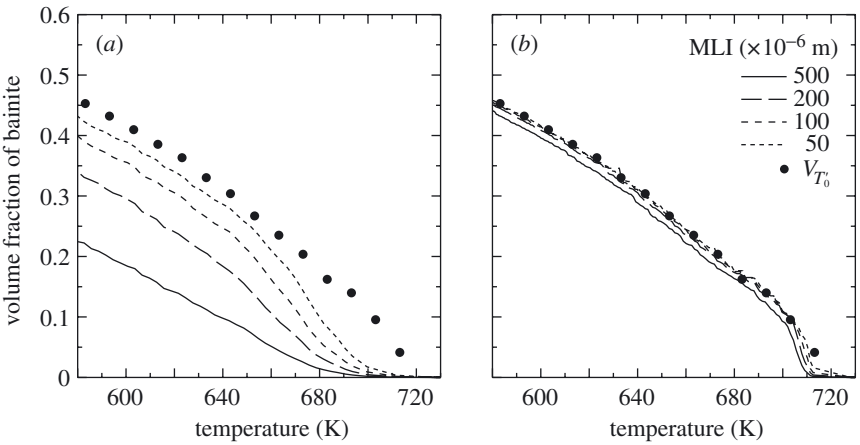

Figure 10. Effect of the austenite grain size on the volume fraction of bainite in continuous cooling transformation. Cooling rates are (*a*) 6.67×10^{-2} K s^{-1} and (*b*) 5.83×10^{-3} K s^{-1}.

The discrepancy between calculated and experimental results may arise from the effect of the non-uniform distribution of carbon in residual austenite. The effect has been examined theoretically, and has indicated that the trapping of carbon in the films of austenite between bainitic ferrite accelerates the bainite transformation (Rees & Bhadeshia 1992*b*). This means that the calculated volume fraction of bainite increases especially at low temperatures if this effect is taken into account in this model, and that it will be more consistent with the experimental results.

In addition, the initial setting of austenite grain size for calculation may affect the agreement because the mean linear intercept was fixed as 86×10^{-6} m in the calculation but the actual austenite grain size just before the start of the transformation should vary with the thermal history within the austenite single-phase region. Figure 10 shows the effect of austenite grain size on the transformation into bainite. It is confirmed that the bainite transformation is retarded as the austenite grain

size increases. It is clear from figure 10 that the transformation is sensitive to the austenite grain size at high cooling rates; at low cooling rates the grain size does not have a large influence simply because the transformation then approaches isothermal conditions. These results suggest that the modelling of the kinetics of the austenite grain growth during cooling is needed in order to predict the transformation kinetics more precisely. Furthermore, a grain-size distribution of austenite may also influences on the difference between the calculated and experimental results. Matsuda & Bhadeshia (2003) presented the overall transformation kinetics model which describes grain-boundary nucleated transformations in the circumstance where the parent-phase grains are not uniform in size, and indicated that the overall transformation rate is fastest when the starting grain is uniform. In this model, the austenite grain size is assumed to be uniform, and therefore the transformation may proceed faster than is observed experimentally.

5. Summary

A theory has been developed to describe the evolution of the bainite reaction in steels, based on the mechanism of solid-state transformation. The model incorporates the early stages of nucleation at austenite grain surfaces, with clusters of platelets (sheaves) forming by the repeated the nucleation of small platelets. The input variables consist of time, temperature, chemical composition and austenite grain size, and it is possible to deal with both isothermal and athermal transformations. Further experimental and theoretical work is needed to allow for the non-uniform distribution of carbon and for the effect of a non-uniform austenite grain size. The methods used in developing the model are in principle applicable to other phases found in steels, such as allotriomorphic ferrite, Widmanstätten ferrite, pearlite and martensite.

The authors are grateful to the NKK Corporation for funding this research and to Professor D. J. Fray for the provision of laboratory facilities at the University of Cambridge, UK.

References

Ågren, J. 1989 A simplified treatment of the transition from diffusion controlled to diffusion-less growth. *Acta Metall.* **37**, 181–189.

Ali, A. & Bhadeshia, H. K. D. H. 1989 Growth rate data on bainite in alloy steels. *Mater. Sci. Technol.* **5**, 398–402

Ali, A. & Bhadeshia, H. K. D. H. 1990 Nucleation of Widmanstätten ferrite. *Mater. Sci. Technol.* **6**, 781–784

Avrami, M. 1939 Kinetics of phase change. I. General theory. *J. Chem. Phys.* **7**, 1103–1112.

Avrami, M. 1940 Kinetics of phase change. II. Transformation-time relations for random distribution of nuclei. *J. Chem. Phys.* **8**, 212–224.

Avrami, M. 1941 Kinetics of phase change. III. Granulation, phase change, and microstructure. *J. Chem. Phys.* **9**, 177–184.

Bhadeshia, H. K. D. H. 1981 A rationalisation of shear transformations in steels. *Acta Metall.* **29**, 1117–1130.

Bhadeshia, H. K. D. H. 1982*a* Bainite: overall transformation kinetics. *J. Phys. Paris* C **43** (Colloq. C4), 443–448.

Bhadeshia, H. K. D. H. 1982*b* Thermodynamic analysis of isothermal transformation diagrams. *Metal Sci.* **16**, 159–165.

Badeshia, H. K. D. H. 1990 Kinetics of the bainite transformation. In *Proc. 6th Int. Conf. Martensitic Transformations, Sydney, Australia, 3–7 July 1989* (ed. B. C. Muddle), Materials Science Forum, vols 56–58, pp. 263–274. Zurich: Trans Tech Publications.

Bhadeshia, H. K. D. H. 1999 Bainite: unresolved issues. *Mater. Sci. Engng* A **273–275**, 58–66.

Bhadeshia, H. K. D. H. 2001 *Bainite in steels*, 2nd edn. London: Institute of Materials.

Bhadeshia, H. K. D. H. & Christian, J. W. 1990 Bainite in steels. *Metall. Trans.* A **21**, 767–797.

Bhadeshia, H. K. D. H. & Edmonds, D. V. 1979 The bainite transformation in a silicon steel. *Metall. Trans.* A **10**, 895–907.

Bhadeshia, H. K. D. H. & Edmonds, D. V. 1980 The mechanism of bainite formation in steels. *Acta Metall.* **28**, 1265–1273.

Caballero, F. G., Bhadeshia, H. K. D. H., Mawella, K. J. A., Jones, D. G. & Brown, P. 2001*a* Design of novel high strength bainitic steels. Part 1. *Mater. Sci. Technol.* **17**, 512–516.

Caballero, F. G., Bhadeshia, H. K. D. H., Mawella, K. J. A., Jones, D. G. & Brown, P. 2001*b* Design of novel high strength bainitic steels. Part 2. *Mater. Sci. Technol.* **17**, 517–522.

Caballero, F. G., Bhadeshia, H. K. D. H., Mawella, K. J. A., Jones, D. G. & Brown, P. 2002 Very strong low temperature bainite. *Mater. Sci. Technol.* **18**, 279–284.

Cahn, J. W. 1956 The kinetics of grain boundary nucleated reactions. *Acta Metall.* **4**, 449–459.

Chang, L. C. & Bhadeshia, H. K. D. H. 1995 Austenite films in bainitic microstructures. *Mater. Sci. Technol.* **11**, 874–881.

Chester, N. & Bhadeshia, H. K. D. H. 1997 Mathematical modelling of bainite transformation kinetics. *J. Physique IV France* **7** (Colloq. C5), 41–46.

Hehemann, R. F. 1970 The bainite transformation. In *Phase transformations. Papers presented at a seminar of the ASM 12–13 October 1968*, ch. 9, pp. 397–432. Metals Park, OH: American Society of Metals.

Hehemann, R. F., Kinsman, K. R. & Aaronson, H. I. 1972 A debate on the bainite reaction. *Metall. Trans.* **3**, 1077–1094.

Johnson, W. A. & Mehl, R. F. 1939 Reaction kinetics in processes of nucleation and growth. *Trans. AIME* **135**, 416–458.

Jones, S. J. 1996 Modelling inclusion potency and simultaneous transformation kinetics in steels. PhD thesis, University of Cambridge, UK.

Jones, S. J. & Bhadeshia, H. K. D. H. 1997*a* Kinetics of the simultaneous decomposition of austenite into several transformation products. *Acta Mater.* **45**, 2911–2920.

Jones, S. J. & Bhadeshia, H. K. D. H. 1997*b* Competitive formation of inter- and intragranularly nucleated ferrite. *Metall. Trans.* A **28**, 2005–2013.

Khan, S. A. & Bhadeshia, H. K. D. H. 1990 The bainite transformation in chemically heterogeneous 300M high-strength steel. *Metall. Trans.* A **21**, 859–875.

Ko, T. & Cottrell, S. A. 1952 The formation of bainite. *J. Iron Steel Inst.* **175**, 307–313.

Magee, C. L. 1970 The nucleation of martensite. In *Phase transformations. Papers presented at a seminar of the ASM in 1968*, ch. 3, pp. 115–156. Metals Park, OH: American Society for Metals.

Matsuda, H. & Bhadeshia, H. K. D. H. 2003 Avrami theory for transformations from non-uniform austenite grain structures. *Mater. Sci. Technol.* **19**, 1330–1334.

Oblak, J. M. & Hehemann, R. F. 1967 Structure and growth of Widmanstätten ferrite and bainite. In *Transformation and hardenability in steels*, pp. 15–33. Ann Arbor, MI: Climax Moly.

Olson, G. B. & Cohen, M. 1976*a* A general mechanism of martensitic nucleation. I. General concepts and the FCC → HCP transformation. *Metall. Trans.* A **7**, 1897–1904.

Olson, G. B. & Cohen, M. 1976*b* A general mechanism of martensitic nucleation. II. FCC → BCC and other martensitic transformations. *Metall. Trans.* A **7**, 1905–1914.

Olson, G. B. & Cohen, M. 1976*c* A general mechanism of martensitic nucleation. III. Kinetics of martensitic nucleation. *Metall. Trans.* A **7**, 1915–1923.

Parker, S. V. 1997 Modelling of phase transformations in hot-rolled steels. PhD thesis, University of Cambridge, UK.

Quidort, D. & Brechet, Y. J. M. 2001 Isothermal growth kinetics of bainite in 0.5% C steels. *Acta Mater.* **49**, 4161–4170.

Rees, G. I. & Bhadeshia, H. K. D. H. 1992*a* Bainite transformation kinetics. Part 1. Modified model. *Mater. Sci. Technol.* **8**, 985–993.

Rees, G. I. & Bhadeshia, H. K. D. H. 1992*b* Bainite transformation kinetics. Part 2. Non-uniform distribution of carbon. *Mater. Sci. Technol.* **8**, 994–996.

Singh, S. B. 1998 Phase transformations from deformed austenite. PhD thesis, University of Cambridge.

Singh, S. B. & Bhadeshia, H. K. D. H. 1996 Quantitative evidence for mechanical stabilisation of bainite. *Mater. Sci. Technol.* **12**, 610–612.

Singh, S. B. & Bhadeshia, H. K. D. H. 1998 Estimation of bainite plate-thickness in low-alloy steels. *Mater. Sci. Engng* A **245**, 72–79.

Thomson, R. C., James, J. S. & Putman. D. C. 2000 Modelling microstructural evolution and mechanical properties of austempered ductile iron. *Mater. Sci. Technol.* **16**, 1412–1419.

Tszeng, T. C. 2000 Autocatalysis in bainite transformations. *Mater. Sci. Engng* A **293**, 185–190.